Role of the Adducted Cation in the Release of Nitroxide End Group of Controlled Polymer in Mass Spectrometry

Michaël Mazarin,[†] Marion Girod,[†] Stéphane Viel,[||] Trang N. T. Phan,[‡] Sylvain R. A. Marque,[§] Stéphane Humbel,[⊥] and Laurence Charles*[,†]

Spectrométries Appliquées à la Chimie Structurale, Chimie Radicalaire, Organique et Polymères de Spécialité, and Structure et Réactivité des Espèces Paramagnétiques, UMR 6264: Laboratoire Chimie Provence, Universités Aix-Marseille I, II, et III−CNRS, F-13397 Marseille, France, and Chimiométrie et Spectrométries and Chimie Théorique et Mécanismes, UMR 6263: Institut des Sciences Moléculaires de Marseille, Aix-Marseille Université−CNRS, F-13397 Marseille, France

Received October 22, 2008; Revised Manuscript Received January 15, 2009

ABSTRACT: The role of cations in the fragmentation of polymer nitroxide labile end groups, as often deplored in matrix-assisted laser desorption/ionization, was investigated. A combination of different spectroscopic techniques and theoretical calculations was implemented to address the mechanistic aspect of the end-group cleavage in a nitroxide-terminated poly(ethylene oxide) macroinitiator agent upon activation in mass spectrometry. When occurring during the ionization process, the homolytic cleavage of a C−ON bond in the end group results in the release of a nitroxide moiety and prevents the intact oligomer from being observed. In contrast, electrospray allowed oligomer ionization in a more gentle process and was used here in conjunction with tandem mass spectrometry to identify factors influencing the release of the end group. Collision-induced dissociation of intact electrosprayed oligomers showed that the elimination of the nitroxide radical depends on the cationizing agent. This fragmentation readily occurs from alkali adducts, whereas it is hardly observed from oligomer adducted with divalent cations such as Cu^{2+}, Zn^{2+}, or Ca^{2+}. Nuclear magnetic resonance experiments actually revealed that the presence of divalent cations in solution would allow the formation of carboxylic salts, inducing an internal proton transfer in the end group. Upon protonation, the C−ON bond dissociation energy increases by about 25 kcal/mol, as indicated by theoretical calculations. This suggests that the release of the nitroxide radical would no longer efficiently compete with alternative dissociation pathways, as observed in MS/MS experiments. On the basis of the structural details provided by NMR and calculations, dissociation mechanisms supported by accurate mass data were proposed to account for all detected fragment ions.

Introduction

Because of their highly ordered nanostructures, block copolymers have become a central component of numerous nanotechnologies.[1−3] Amphiphilic copolymers, consisting of hydrophilic and hydrophobic blocks, are industrially significant because of their biological and chemical properties.[4] More specifically, amphiphilic block copolymers containing poly(ethylene oxide) (PEO) as the hydrophilic segment were prepared for prospective use in many applications, such as stabilizers,[5,6] templates for the elaboration of inorganic nanoparticules,[7,8] electrolytes for rechargeable lithium batteries[9,10] or compatibilizers in polymer blending.[11−13] The performance of block copolymer materials highly depends on structurally related parameters, such as molecular weight distribution, chemical nature of the end groups, and balance between hydrophobic and hydrophilic segments. Well-defined structure copolymers can be synthesized, on both a laboratory and an industrial scale, using controlled radical polymerization (CRP) techniques.[14] The functionalization of PEO usually serves as a preliminary step for the preparation of smart functional materials. To synthesize PEO-based block copolymers, the introduction of an appropriated functional initiator at the α-, ω-, or both chain ends is quantitatively, or near quantitatively, necessary. Depending on the CRP method used, nitroxide, halogen, or dithioester groups were grafted onto the PEO chain ends, and the PEO-based macroinitiator agents were then used for the CRP of the targeted monomer. Therefore, precise structural determination of the end groups is an important issue for subsequent reaction of the PEO-based macroinitiator agents as well as for the elucidation of mechanistic details. To gain information on both the structure and the molecular weight of the PEO-based macroinitiator agents, it is essential to select a technique that avoids the decomposition of the labile end groups.

Since the development of soft ionization techniques, mass spectrometry (MS) has become a powerful tool for living polymer analysis.[15] In particular, matrix-assisted laser desorption/ionization (MALDI) time-of-flight (ToF) MS has been shown to be applicable to more types of synthetic polymers than any other MS techniques and generally leads to spectra that display singly charged oligomers with little or no fragmentation. However, in the case of fragile end-group polymers, cleavage of terminal moieties may easily occur upon ionization, and gas-phase ions produced by MALDI are no longer intact polymer adducts.[16−18] Such results were already deplored in MALDI analysis of polymers obtained via nitroxide mediated polymerization (NMP)[19−22] or reversible addition−fragmentation chain transfer (RAFT) polymerization.[18,23−25] The use of acidic matrices to promote selective protonation of labile nitroxide end groups was reported to be an efficient way to prevent these undesired fragmentations.[20] Alternatively, selective protonation of small living PEO oligomers in MALDI could be afforded using a solvent-free preparation method to avoid alkali contaminants from the solvents.[22] However, the need for protonation

* Corresponding author. Tel: +33 4 91 28 86 78. Fax: +33 4 91 28 28 97. E-mail: laurence.charles@univ-provence.fr.
[†] Spectrométries Appliquées à la Chimie Structurale, UMR 6264: Laboratoire Chimie Provence, Universités Aix-Marseille I, II, et III−CNRS.
[‡] Chimie Radicalaire, Organique et Polymères de Spécialité, UMR 6264: Laboratoire Chimie Provence, Universités Aix-Marseille I, II, et III−CNRS.
[§] Structure et Réactivité des Espèces Paramagnétiques, UMR 6264: Laboratoire Chimie Provence, Universités Aix-Marseille I, II, et III−CNRS.
[||] Chimiométrie et Spectrométries, UMR 6263: Institut des Sciences Moléculaires de Marseille, Aix-Marseille Université−CNRS.
[⊥] Chimie Théorique et Mécanismes, UMR 6263: Institut des Sciences Moléculaires de Marseille, Aix-Marseille Université−CNRS.

10.1021/ma802372m CCC: $40.75
Published on Web 02/20/2009

Scheme 1. Synthesis of a Poly(ethylene oxide) (PEO) Functionalized with a 2-Methyl-2-[*N-tert*-butyl-*N*-(1-diethoxyphosphoryl-2,2-dimethyl propyl)aminoxy]propanoic acid (MAMA-SG1)[a]

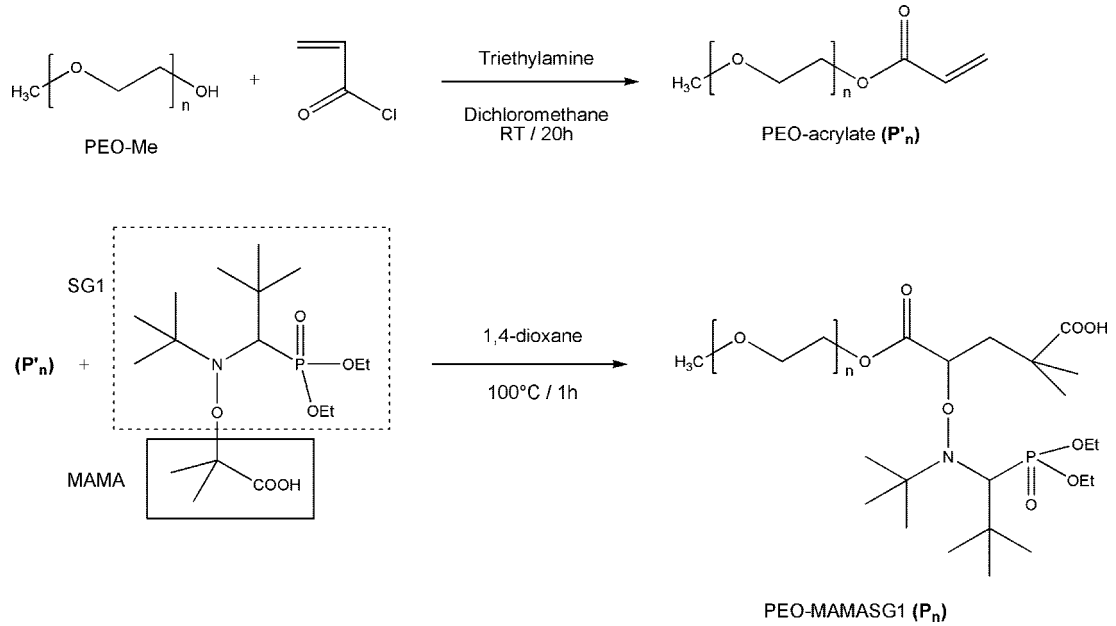

[a] First step consists of the preparation of acrylate-termined PEO (PEO−acrylate, P'_n) from a methoxy-terminated PEO, and the second step is the intermolecular radical addition of MAMA-SG1 alkoxyamine onto P'_n Here the functionalized P_n polymer is named PEO-MAMASG1.

to prevent fragmentation of labile end groups in MALDI has never been clearly elucidated. Furthermore, in contrast with low-mass analytes or biopolymers, MALDI of most synthetic polymers preferentially occurs through cationization rather than protonation.[26]

To find out whether some special experimental conditions are to be used in MALDI to avoid this undesired spontaneous dissociation, a better knowledge of factors that influence the release of the end group is necessary. In particular, the role of the cation adducted to the molecules during the ionization step needs to be better understood. Electrospray ionization (ESI) is an alternative technique for studying macromolecules by MS. Although ESI is less widely used than MALDI for synthetic polymers because of a more limited molecular-weight application range, this ionization technique is known to be more gentle and, in contrast with MALDI, was shown to allow fragile end-group polymers to be produced as intact cationized adducts in the gas phase.[27−29] As a result, ESI is particularly appropriate for generating intact ionized oligomers for which fragmentation behavior could be further studied under controlled conditions during collision-induced dissociation (CID) experiments. This approach would allow the ionization and the dissociation steps to occur sequentially, and although ion activation would not occur by the same means, obtained results should be useful to shed light on dissociation mechanisms as observed to occur in the MALDI source.

Here we proposed to investigate the influence of cations on the cleavage of the fragile end group of a PEO-based macroinitiator agent by submitting electrosprayed oligomers to CID. This PEO was functionalized with a MAMA-SG1 end group, namely, acid 2-methyl-2-[*N-tert*-butyl-*N*-(1-diethoxyphosphoryl-2,2-dimethyl propyl)aminoxy] propanoic (Scheme 1). This so-called PEO-MAMA-SG1 was chosen in this study because preliminary experiments had shown that the same bond cleavage in the ω-end group, that is, the release of the SG1 nitroxide moiety as a radical, was observed during MALDI or CID.[22,29] Results indicate that this C−ON bond cleavage was not observed during CID of $[M + C^{II}]^{2+}$ ions, that is, oligomers cationized with divalent C^{II} cations. A multidisciplinary approach involving NMR experiments and theoretical calculations revealed that the undesired bond homolysis was actually prevented by protonation of the N atom, which was favored in solution by a proton transfer induced by divalent cations.

Experimental Section

Materials and Reagents. HPLC grade methanol was purchased from SDS (Peypin, France). All chemicals were from Sigma-Aldrich (St. Louis, MO) and were used as received. For MS experiments, PEO-MAMASG1 was first dissolved in methanol and further diluted using methanolic salt solutions to a final 57 μg mL^{-1} concentration. HCOOH, LiI, NaI, KI, RbI, CsI, $Ca(NO_3)_2$, $CuCl_2$, and $ZnCl_2$ were all used at a 1 mM concentration. CD_3OD solvent used in NMR experiments was from Euriso-Top (Saint-Aubin, France).

PEO-MAMASG1 Synthesis. The synthesis procedure of PEO-MAMASG1 ($\mathbf{P_n}$) involves two steps including the preparation of PEO−acrylate ($\mathbf{P'_n}$) and the intermolecular radical addition of MAMA-SG1 alkoxyamine to $\mathbf{P'_n}$, as shown in Scheme 1. In a three-necked round-bottomed flask equipped with a water-cooled condenser, methoxy PEO of molar mass of 350 g mol^{-1} (10.0 g, 28.6 mmol) and triethylamine (16 mL, 114.3 mmol) were mixed in 180 mL of CH_2Cl_2. The solution was flushed with N_2 for 15 min and cooled to 5 °C; then, 9.7 mL (114.3 mmol) of acryloyl chloride in 20 mL of CH_2Cl_2 was added dropwise under dry nitrogen. After this addition was complete, the reaction solution was allowed to warm to room temperature, and the reaction mixture was stirred overnight. The solvent CH_2Cl_2 was removed by rotary evaporation, and 100 mL of ethyl acetate was added to it. The syrup precipitated of triethylammonium chloride was filtered off. Ethyl acetate was removed by rotary evaporation. The viscous residue was dissolved in 150 mL of CH_2Cl_2 and washed three times with 30 mL of saturated $NaHCO_3$ solution. The product was dried over $MgSO_4$, and the solvent was removed by rotary evaporation. The methoxy poly(ethylene oxide)−acrylate (MePEO−acrylate or $\mathbf{P'_n}$) was then precipitated in cold *n*-hexane, isolated by filtration, and dried under reduced pressure to a constant mass. ^{1}H NMR ($CDCl_3$, 300 MHz, δ): 3.38 (s, 3H, CH_3O), 3.65 (s, 33H, CH_2), 4.32 (dd, 2H, CH_2OCO), 5.86, 6.17, and 6.40 (d, dd, d, 3H, CH_2═CH). One of the vinyl protons of the acrylate group in $\mathbf{P'_n}$ could be observed by ^{1}H NMR at δ 6.40−6.45. The reaction yield of this first step (9.8

g, 85%) was determined by comparing the integration of this proton peak and the CH_3 α-end group protons (δ 3.38).

In a two-necked round-bottomed flask equipped with a water-cooled condenser, MePEO−acrylate (0.5 g) was then mixed with 6 mL of THF. The BlocBuilder (1.2 g) was then added to the solution. After complete dissolution, the mixture was deoxygenated by nitrogen bubbling for 20 min; then, the reaction was performed at 100 °C for 1 h. The solution was then cooled in an ice water bath and precipitated in cold diethyl ether. It was then filtered, washed with cold diethyl ether, and dried under vacuum to a constant mass. The reaction yield was found to be 85%. ^{1}H NMR ($CDCl_3$, δ): 4.57 (dd, 1H, J = 3.22 Hz, J = 11.75 Hz, CHO), 4.38−3.83 (m, 6H, CH_2OCO and CH_2OP), 3.64 (s, 33H, CH_2), 3.38 (s, 3H, CH_3O), 3.34 (d, 1H, J= 26.12 Hz, N−CH−P), 2.53 (dd, 1H, J = 3.21 Hz, J = 14.16 Hz, CH_2), 2.32 (dd, 1H, J = 12.27 Hz, J = 13.76 Hz, CH_2), 1.45−1.22 (m, 12H, CH_3), 1.17 (s, 9H, CH_3), 1.08 (s, 9H, CH_3). The ^{1}H NMR spectrum of the PEO-MAMASG1 also shows that the signals due to the vinyl protons of the acrylate group (δ 5.75−6.45) disappear, indicating that no residual MePEO−acrylate was present in the sample.

Mass Spectrometry. All experiments were performed with a QStar Elite mass spectrometer (Applied Biosystems SCIEX, Concord, ON, Canada) equipped with an ESI source operated in the positive ion mode. The capillary voltage was set at 5500 V, and the cone voltage was set at 30 V. In this hybrid instrument, ions were measured using an orthogonal acceleration time-of-flight (oa-TOF) mass analyzer. A quadrupole was used for selection of precursor ions to be further submitted to CID in MS/MS experiments. Nitrogen was used as the nebulizing gas (20 psi), the curtain gas (20 psi), and the collision gas. Collision energy was set according to the experiments. Analyst software version 2.1 was used for instrument control, data acquisition, and data processing. Direct sample introduction was performed at a 5 μL min^{-1} flow rate using a syringe pump.

Nuclear Magnetic Resonance Spectroscopy. All NMR experiments were recorded on a 500 MHz Bruker Avance spectrometer with a 5 mm triple-resonance broadband inverse ^{1}H/X/^{31}P Bruker probe head equipped with an actively shielded z-gradient coil. All solutions for NMR analyses were prepared by properly diluting calculated amounts of stock solutions directly into the NMR sample tubes, leading to a solution volume of about 0.6 mL. ^{1}H experiments were acquired at a nominal ^{1}H Larmor frequency of 500.13 MHz. A simple one-pulse sequence was used with a 90° pulse length of 7.5 μs. ^{13}C{^{1}H} experiments were recorded at a nominal ^{13}C Larmor frequency of 125.75 MHz using WALTZ-16 ^{1}H decoupling as well as low-power ^{1}H irradiation during the ^{13}C relaxation delay to ensure NOE enhancement. The 90° pulse for ^{13}C was 10.5 μs. The ^{1}H and ^{13}C NMR assignments of compounds $\mathbf{P_n}$ and **X** (Figure 5) were obtained using a series of 2D gradient-selected NMR experiments (^{1}H−^{1}H COSY, ^{1}H−^{13}C HSQC, ^{1}H−^{13}C HMBC) for which conventional acquisition parameters were used, as described in the literature.[30]

Nuclear Magnetic Resonance Diffusion Experiments. Pulsed gradient spin echo (PGSE) experiments[31−33] were performed on the same spectrometer and probe head as that described above. We calibrated the gradient coil constant of the probe head by measuring the self-diffusion coefficient of the residual proton in 99.9% D_2O,[32] and it was found to have a maximum strength of 56 G cm^{-1}. The temperature was set and controlled to 300 K with an air flow of 545 L h^{-1} to minimize temperature gradients and to avoid temperature fluctuations due to sample heating during the gradient pulses. The pulse sequence was based on the stimulated echo and incorporated bipolar gradient pulses and a longitudinal eddy current delay (BPP-LED)[34] to minimize spectral artifacts resulting from eddy currents. In this case, the amplitude of an NMR resonance observed at the echo is given by

$$I = I_0 \exp(-D(\gamma g \delta)^2(\Delta - \varepsilon(\delta))) \quad (1)$$

where I_0 is the resonance amplitude at zero gradient strength, D is the self-diffusion coefficient of the molecule, γ is the magnetogyric ratio of the observed nucleus, g and δ are the strength and the duration of the gradient pulses, respectively, and Δ is the diffusion time, that is, the time during which the diffusion is monitored. The correction factor $\varepsilon(\delta)$ depends on both δ and the pulse sequence. Note that strictly speaking the I_0 term given in eq 1 is an implicit function of the NMR relaxation times T_1 and T_2. Usually, all delays are kept constant to avoid any complication arising from magnetic relaxation, and only the gradient strength is varied.[31] Specifically, the gradient strength was quadratically incremented in 16 steps from

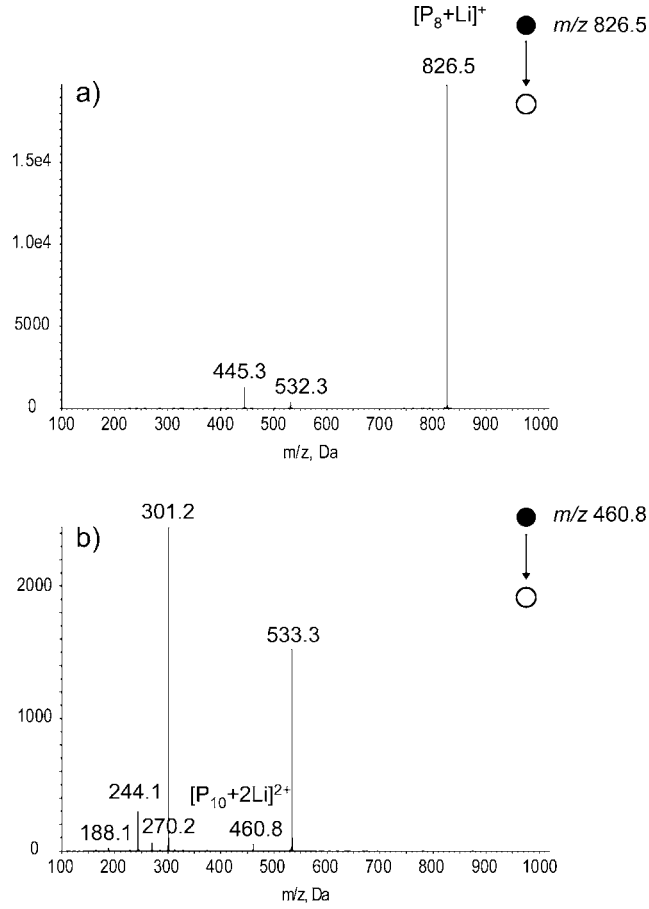

Figure 1. Electrospray tandem mass spectrometry spectra of (a) singly lithiated 8-mer, $[P_8 + Li]^+$, at m/z 826.5 and (b) doubly lithiated 10-mer, $[P_{10} + 2Li]^{2+}$, at m/z 460.8, acquired at a 0.50 eV collision energy (center-of-mass).

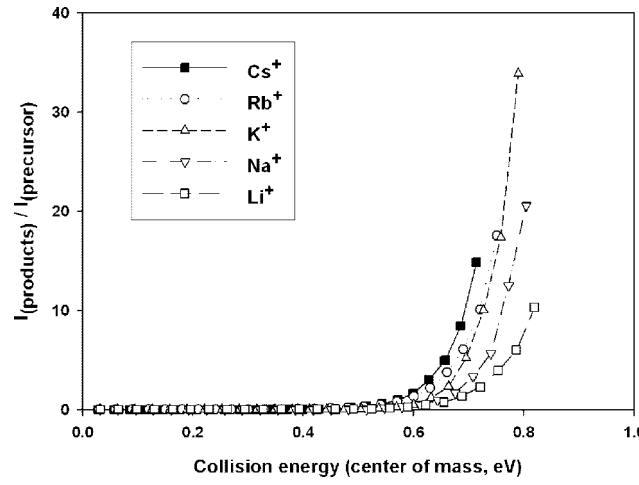

Figure 2. Intensity ratio of product ions versus precursor ion in MS/MS of singly cationized 8-mer, $[P_8 + C]^+$, with C = Li, Na, K, Rb, and Cs, as a function of collision energy (center-of-mass).

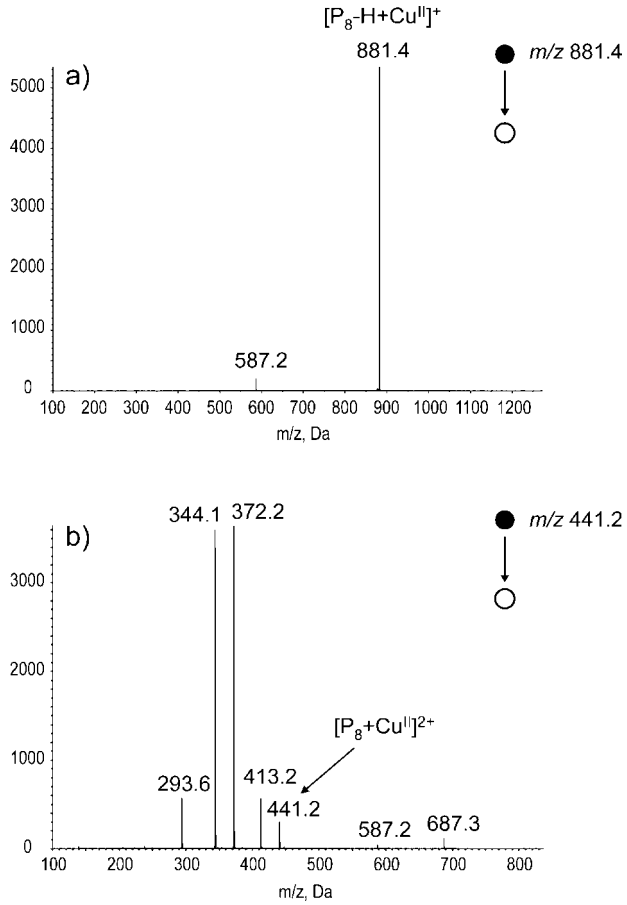

Figure 3. Electrospray tandem mass spectrometry spectra of (a) copper adduct of the deprotonated 8-mer, $[P_8-H+Cu^{II}]^+$, at *m/z* 881.4 and (b) copper adduct of the 8-mer, $[P_8+Cu^{II}]^{2+}$, at *m/z* 441.2, acquired at a 0.30 eV collision energy (center-of-mass).

6 to 95% of its maximum value. The diffusion time (100 ms) and the duration of the sine-shaped gradient pulses (1.2 ms) were optimized to achieve a 95% decrease in the resonance intensity of the slowest diffusing species, whereas the delays allotted to the decay of the eddy current and to the gradient pulse recovery were set to 25 and 0.1 ms, respectively. After Fourier transformation and phase correction, the baseline of the spectra was carefully adjusted. We analyzed the data by plotting the signal intensities (areas) as a function of the gradient strength and fitting the resulting decay curves to eq 1 using a nonlinear least-squares fit based on the Levenberg−Marquardt algorithm. All decays were strictly monoexponential.

Computational Details. Geometry optimizations were performed at the B3LYP/6-31G(d) level, as implemented into Gaussian 03 revision C.02.[35] Additional single-point energies were obtained with the more extended cc-pvtz[36,37] basis set and the MP2 approximation. Although spin contamination of the radicals was usually small in all of this study, we systematically use spin projected values (PMP2).

Results and Discussion

Alkali Cations. Using alkali as cationizing agents, ESI of PEO-MAMASG1 ($\mathbf{P_n}$) produced both singly and doubly charged oligomer adducts with $n = 3$ to 14 and $n = 8$ to 22, respectively. The use of lithium was shown to generate two envelopes of similar intensities, whereas the +1 distribution was the most intense one with other alkali. (See the Supporting Information.) The influence of the adducted cation on the oligomer MS/MS behavior was studied for both charge states. As the most abundant ion in the +1 distribution, the singly charged 8-mer, noted $[\mathbf{P_8} + C]^+$ with C = Li, Na, K, Rb, or Cs, is presented here as an illustrating example. CID of the lithiated 8-mer (*m/z* 826.5) obtained at a center-of-mass collision energy of 0.50 eV produced two main fragment ions (Figure 1a). The peak observed at *m/z* 532.3 would arise from the loss of a 294.2 Da radical moiety from the precursor ion. According to accurate mass measurements, this radical would be the SG1 nitroxide, released after homolytic cleavage of the C−ON bond within the ω-end group.[22,29] The thermal unstability of the C−ON bond within the ω-end group of the PEO-MAMASG1 is the basis of the NMP process. The same homolytic cleavage would then occur upon the CID process and was advantageously used in a recent MS/MS study to characterize the PS block size in a SG1-terminated PEO-*b*-PS copolymer.[29] The so-obtained *m/z* 532.3 odd-electron ion would then readily further dissociate via the release of a second radical,[22] named MAMA•, to yield the fragment ion detected at *m/z* 445.3 (*m/z* 445.2619; error, −7.1 ppm), which has the same structure as a lithiated acrylate-terminated 8-mer ($\mathbf{P'_8}$). Although the use of Li^+ as the adducting cation is well-known for promoting the most informative MS/MS reactions of PEOs by inducing specific backbone fragmentation reactions,[38,39] no other fragment ions could be detected in this MS/MS spectrum. An increase in collision energy above 0.80 eV (center-of-mass) was required to generate additional peaks in the 100−440 *m/z* range. These very low abundance ions could be assigned to fragment ions from the A, B, C, and D series described by Lattimer[38,40] and Chen,[41] arising from the dissociation of the lithiated acrylate-terminated 8-mer ($\mathbf{P'_8}$) at *m/z* 445.3. Similar results were obtained using the other alkali as cationizing agents. This result is in great contrast with usually reported data that show that by using all alkali but lithium, dissociation of cationized PEO mainly proceeds via the release of the bare metal ion.[38,39,41−46] This suggests that the energy required for the homolytic cleavage of the C−ON bond in the MAMASG1 end group is lower than the binding energy of the cation to the oligomer. By plotting the intensity ratio of product ions versus precursor ion as a function of collision energy, it can be seen that the two main reactions proceed from very low energies (Figure 2). Although the dissociation energy threshold could not be accurately measured with the instrument used in this study, data from Figure 2 indicate that the energy required to promote these homolytic cleavages decreases as the cation size increases. The observed relative stability of the different ionized oligomers as a function of the adducted cation would be consistent with previously reported data, indicating the strength of interactions within the ionic adduct increases as the cation size decreases.[38,40−45]

Doubly charged oligomer adducts were also submitted to CID, as exemplified in Figure 1b with the MS/MS spectrum obtained for $[\mathbf{P_{10}} + 2Li]^{2+}$ (*m/z* 460.8). In contrast with singly charged adducts, doubly lithiated precursors were observed to undergo more extensive dissociations, giving rise to fragment ions of high abundance. The two successive radical eliminations, that is, SG1• and MAMA•, were also observed to proceed from doubly charged precursors, producing the final acrylate-terminated PEO ($\mathbf{P'_{10}}$) as a singly and a doubly lithiated adduct, respectively, detected at *m/z* 533.3 and 270.2. These assignments were supported by accurate mass measurements. The radical cations formed after the SG1• release, expected at *m/z* 620.3 in the +1 charge state and at *m/z* 313.7 as a doubly lithiated adduct, could not be observed in the MS/MS spectrum, which suggests that they further dissociate via the elimination of MAMA• in a fast process. Nevertheless, the validity of the proposed mechanism was supported by the presence of an intense peak at *m/z* 301.2, which could be attributed to $[SG1• + Li]^+$ on the basis of accurate mass measurements (*m/z* 301.1988; error, −25.2 ppm). The size of the error associated with mass measurements

Scheme 2. Proposed Fragmentation Mechanism of *m/z* 301.2 to Yield *m/z* 244.1, Which Further Dissociates to Produce *m/z* 188.1

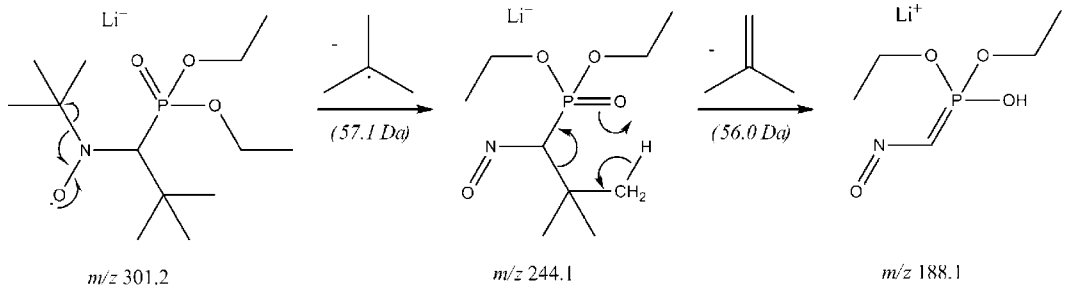

in MS/MS spectra can be relatively large because it is highly dependent on the relative response of the target and the reference peaks, and accuracy is further altered when these ions are not in the same charge state.[47] The higher abundance of singly charged fragment ions (*m/z* 533.3 and 301.2) as compared with *m/z* 270.2 could suggest that one of the lithium cation would preferentially be located on the MAMASG1 end group at the time of the fragmentation. Alternatively, this result could indicate that the adduction of Li^+ on the end group would favor SG1• release from the precursor ion. Two additional peaks were detected at *m/z* 244.1 and 188.1. As indicated by accurate mass measurements (*m/z* 244.1285; error, −9.6 ppm), elimination of a *tert*-butyl radical would proceed from *m/z* 301.2 (Scheme 2), as previously reported in the literature.[48] Consecutively, the loss of a 2-methylprop-1-ene molecule from *m/z* 244.1 would account for the formation of *m/z* 188.1 (*m/z* 188.0659; error, −9.3 ppm). MS/MS experiments performed on $[\mathbf{P_{10}} + 2C]^{2+}$, with C = Na, K, Rb, and Cs, gave rise to the same fragmentation pattern as that observed for the doubly lithiated adduct. As previously noticed for singly charged oligomers, the rate of radical eliminations from $[\mathbf{P_{10}} + 2C]^{2+}$ was shown to increase with the cation size. However, in contrast with the case of Li^+, a competing MS/MS reaction was observed to produce the bare alkali cation.

Divalent Cations. Copper, calcium, and zinc were tested to promote PEO-MAMASG1 ESI. Using Cu^{2+} as the cationizing agent, two main distributions were obtained and could be assigned to $[\mathbf{P_n}-H + Cu^{II}]^+$ (n = 2 to 13) and $[\mathbf{P_n} + Cu^{II}]^{2+}$ (n = 5 to 17) oligomer adducts. In contrast with MS data usually obtained with such a transition-metal ion,[49] no species indicating the reduction of Cu(II) to Cu(I) during the ESI process could be detected. Similar MS data were obtained when using other divalent ions such as Ca^{2+} or Zn^{2+}. Both types of oligomer copper adducts were submitted to CID experiments. Figure 3 displays MS/MS spectra of $[\mathbf{P_8}-H + Cu^{II}]^+$ (*m/z* 881.4) and $[\mathbf{P_8} + Cu^{II}]^{2+}$ (*m/z* 441.2) acquired at the same center-of-mass collision energy (0.30 eV). From the singly charged precursor ion, one main low-abundance ion was produced at *m/z* 587.2 (Figure 3a), corresponding to the release of SG1• from $[\mathbf{P_8}-H + Cu^{II}]^+$, as supported by accurate mass measurements (*m/z* 587.2123; error, −2.4 ppm). In contrast with data obtained from oligomer alkali adducts, the consecutive loss of MAMA• could not be observed, although collision energy was raised. Dissociation of $[\mathbf{P_8} + Cu^{II}]^{2+}$ (*m/z* 441.2) produced more fragment ions, some of which were particularly abundant (Figure 3b). Interestingly, none of the detected fragment ions indicated the release of SG1• or SG1• and MAMA•. Similar results were also obtained using Ca^{2+} or Zn^{2+}, suggesting a particular role of divalent cations C^{II} in preventing the undesired homolytic cleavage of the C−ON bond from $[PEO\text{-}MAMASG1 + C^{II}]^{2+}$. Peak assignment in these two MS/MS spectra is further addressed below by reference to structural data provided by NMR and theoretical calculations.

Binding Site of Divalent Cations in MAMA-SG1 End Group. The effects of the groups attached to the C−ON group as well as the effect of the surroundings on the strength of the C−ON bond have been extensively studied. In particular, it was reported that increasing the polarity of the group attached to the carbon atom would increase the homolysis rate constant,[50] that is, a C−ON bond weakening effect, whereas the opposite behavior was observed for the nitrogen atom.[51] Furthermore, the formation of carboxylic salts on the alkyl fragment was further suspected to play a role in the strength of the C−ON bond.[52] This homolysis reaction was also shown to depend highly upon the nature of the released radical, a stabilized (π-type) versus a nonstabilized (σ-type) alkyl radical.[53] Considering the enol form of the end group, two hydroxyl functions (one from the enol and one from the carboxylic acid group) would be available to chelate Cu^{2+}. The possibility for such a keno−enolic equilibrium to be displaced toward the enol form in the presence of copper was thus investigated. Such a shift toward one tautomeric form over the other one has already been observed for the imidazolic ring.[54] Homolytic cleavage of the weak C−ON bond would yield a σ radical moiety from the

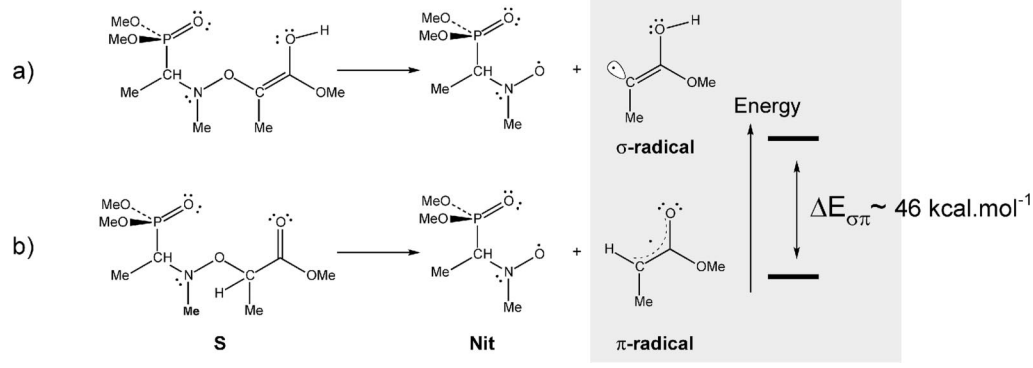

Figure 4. Energy difference ($\Delta E_{\sigma\pi}$) between the σ radical, formed from the enol form, and π radical, formed from the keto form, as calculated in a model system (**S**). See Table 1.

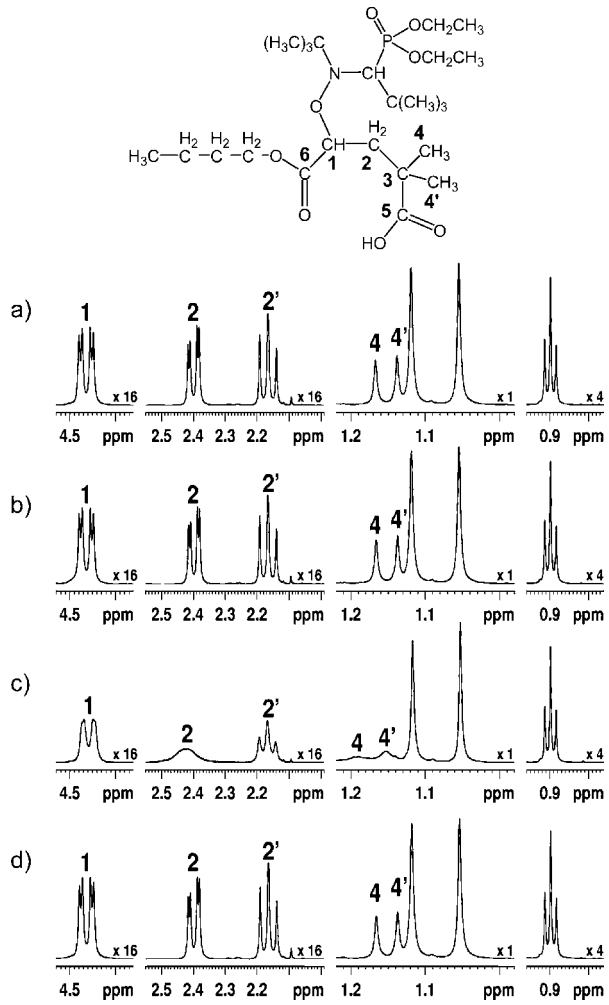

Figure 5. Selected regions of the 500 MHz ^{1}H NMR spectra of **X** at a 20 mM concentration in methanol-d_4 and recorded at 300 K (a) without added salt and with 20 mM added (b) KCl, (c) $CuCl_2$, and (d) $ZnCl_2$. Because the spectral line width is slightly larger in c than in all of the other spectra, as a result of the presence of the paramagnetic Cu^{2+} ions in solution, the spectra in a, b, and d were processed with a 1 Hz exponential line broadening, whereas no apodization function was used in c. This allowed us to normalize the nonspecific increase in line width observed in c somehow, as shown by the methyl group spectral regions reported on the right-hand side, which exhibit similar line widths in all of the spectra. In this way, the strong selective line broadenings observed for H-**1**, H-**2**, H-**2′**, H-**4**, and H-**4′**, are clearly evidenced. Note that in c a slight chemical shift displacement (+0.06 ppm) was observed for all of the ^{1}H signals. This shift was purposely accounted for by setting the ^{1}H chemical of the terminal methyl group of the butyl moiety to 0.9 ppm, that is, the same value as that observed for this signal in all of the other cases, to aid in the spectral comparison. Such shift was also observed for compound $\mathbf{P_n}$ when adding Cu^{2+} ions in solution but was never observed when adding Zn^{2+}, for neither **X** nor $\mathbf{P_n}$.

Table 1. Absolute Energies (in Hartree) of the σ Radical, Formed from the Enol Form, and π Radical, Formed from the Keto Form, As Calculated in a Model System (S)[a]

method	π radical	σ radical	$\Delta E_{\sigma\pi}$
B3LYP[b]	−307.04844	−306.96722	51.0
MP2[c]	−306.46905	−306.39256	48.0
PMP2[c]	−306.47417	−306.39995	46.6
MP3[c]	−306.49854	−306.42635	45.3
CCSD[c]	−306.50915	−306.43722	45.1
CCSD(T)[c]	−306.55719	−306.48493	45.3

[a] Energy differences ($\Delta E_{\sigma\pi}$) are in kcal/mol. The geometry is optimized at the B3LYP/6-31G(d) level. [b] Basis set: 6-31G(d). [c] Basis set: cc-pvtz.

enol, whereas a π radical could be produced from the keto form (Figure 4). The ability to eliminate SG1• upon CID might thus depend on the stability of the so-formed complementary radical. Calculations performed on a model system (**S**) indicate that at the PMP2/cc-pvtz level, the σ radical was energetically less favored than the π radical by about 46 kcal/mol (Figure 4 and Table 1). Such a large difference is to be attributed to the π delocalization that stabilizes the π radical and should not be greatly modified by σ-substituant effects, so this value obtained in a model should be very similar to that of the real system. This energy difference is slightly overestimated at the B3LYP level, so PMP2 values seem to be a good compromise between computational cost and accuracy (Table 1). For the next part, we chose to use the PMP2/cc-pvtz values as obtained on B3LYP/6-31G(d) optimized geometries.

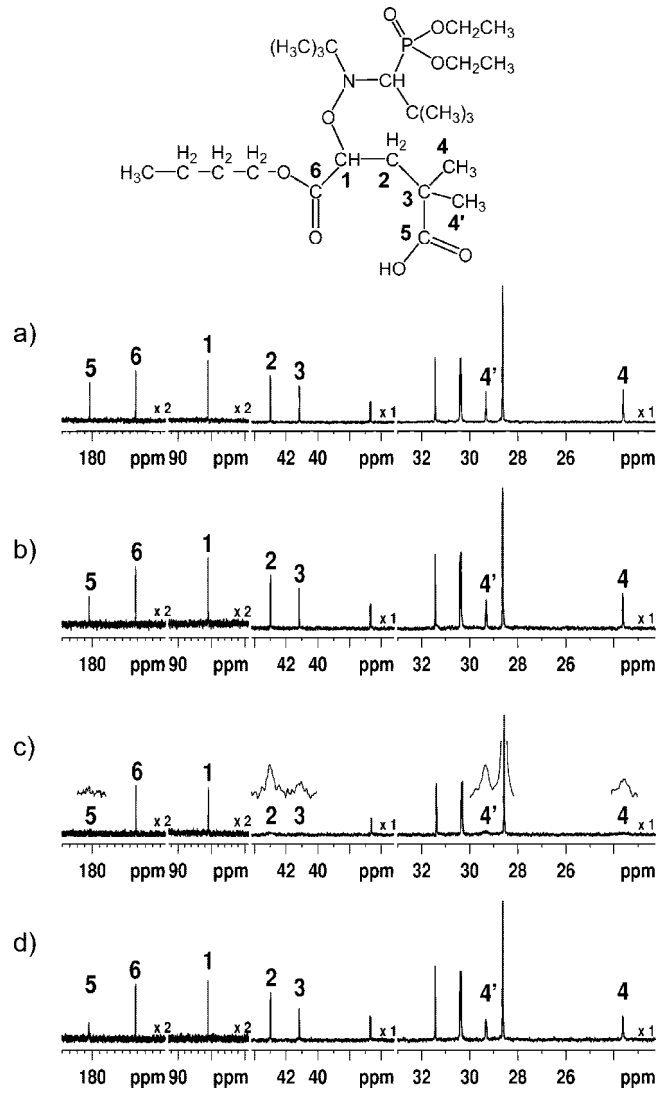

Figure 6. Selected regions of the 125 MHz $^{13}C\{^1H\}$ NMR spectra of **X** at 20 mM concentration in methanol-d_4 and recorded at 300 K (a) without added salt and with 20 mM added (b) KCl, (c) $CuCl_2$, and (d) $ZnCl_2$. All spectra were processed with a 1 Hz exponential line broadening prior to Fourier transformation. In c, the gray portions of the curve correspond to specific regions of the same spectrum but were processed with a 12 Hz exponential line broadening to detect the presence of broad signals. Moreover, as in Figure 5, a slight chemical shift displacement (+0.06 ppm) was observed for all of the ^{13}C signals in c but was not compensated for because it was insignificant when compared to the large ^{13}C chemical shift range involved.

To evidence any keto−enol tautomeric equilibrium of PEO-MAMASG1, high-resolution NMR experiments were performed on a model compound terminated with the same MAMASG1 end group and that behaved similarly to $\mathbf{P_n}$. This compound, hereafter referred to as **X**, was initially preferred to $\mathbf{P_n}$ because

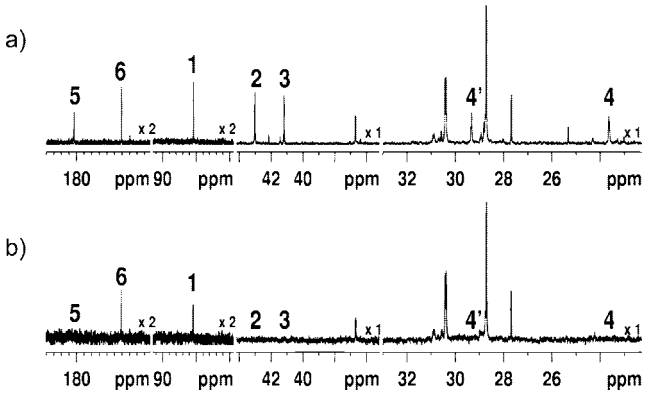

Figure 7. Selected regions of the 125 MHz $^{13}C\{^1H\}$ NMR spectra of $\mathbf{P_n}$ at 20 mM concentration in methanol-d_4 and recorded at 300 K (a) without and (b) with 20 mM added $CuCl_2$.

Table 2. Self-Diffusion Coefficients Obtained by PGSE NMR Experiments at 300 K on 20 mM Methanol-d_4 Solutions of X Containing Added Salts at 20 mM[a]

sample	$D_{\mathbf{X}}$ ($\times 10^{-10}$ m^2 s^{-1})	D_{TMS} ($\times 10^{-9}$ m^2 s^{-1})	$(a_X^{salt})/(a_X^{ref})$
X	7.30	2.11	
X + $CuCl_2$	7.17	2.15	1.04[b]
X + $ZnCl_2$	7.21	2.12	1.02[b]
X + KCl	7.21	2.13	1.02[b]

[a] All solutions also contained a trace amount of TMS used as an internal standard. [b] Given at ± 5%.

it was readily available. Specifically, ^1H NMR experiments were recorded on a series of methanol-d_4 solutions of **X** at 20 mM with K^+, Cu^{2+}, and Zn^{2+} added at 20 mM (Figure 5). This gave a final cation/X ratio of 1:1, similar to the one commonly used in MS. The ^1H spectra of all of these solutions were almost perfectly identical, except for the spectrum recorded in the presence of the Cu^{II} ions which showed relatively broadened ^1H resonances due to the presence in solution of the paramagnetic Cu^{II} species.[55] Overall, no signal due to the enol form could be detected, and the integrals of the NMR signals were consistent with the presence in solution of only the keto form because the relative integral of the CH-**1** signal was equal to 1, as expected.

Interestingly, a closer look at the ^1H spectra revealed a selective line broadening of some of the ^1H resonances in the ^1H spectrum recorded in the presence of the Cu^{II} ions, as shown in Figure 5. To clarify this point, proton decoupled ^{13}C NMR experiments were also recorded on the same solutions, and the corresponding spectra are reported in Figure 6. As can be seen in this Figure, the $^{13}C\{^1H\}$ signals due to carbon atoms C-**5**, C-**2**, C-**3**, C-**4**, and C-**4′**, of compound **X** were also strongly enlarged in the presence of the Cu^{II} ions, as evidenced by the inserted gray trace reported in Figure 6c. The strong selective line broadenings observed upon the addition of Cu^{II} were attributed to the large enhancement of transverse relaxation rates due to the dipolar coupling between the copper unpaired electron and the ^1H and ^{13}C magnetic moments of the **X** nuclei.[55] Because of the local aspect of the dipolar interaction, which varies as $1/r^6$, where r is the distance between the unpaired electron and the considered nuclear spins, the selective line broadening informs about the complexation site and the respective location of Cu^{II} with respect to the various nuclear spins. In this respect, the observation of selective ^1H and ^{13}C line broadenings for CH_2-**2**, C-**3**, CH_3-**4**, CH_3-**4′**, and CO-**5** as well as the concomitant absence of any line broadenings for the CO-**6** resonance strongly suggest that the Cu^{II} ions interact with this specific moiety of the molecule and bind to the hydroxyl function of the carboxylic group. Similar results were obtained for $\mathbf{P_n}$, as shown in Figure 7. The situation was somewhat different in the case of the Zn^{II} ions, which are not paramagnetic. However, it is well known that upon complexation, the chemical shift of the nuclei in the proximity of the metal center can be modified because of the corresponding change in the local electronic density brought

Table 3. Energetics for the Modification of the C−ON Bond Dissociation Energy (BDE) During Protonation[a]

	absolute energies (au)		relative energies (kcal/mol)	
species	B3LYP[b]	PMP2[c]	B3LYP[b]	PMP2[c]
σ radical	−306.96722	−306.39995	0.0	0.0
π radical	−307.04844	−306.47417	−51.0	−46.6
Nit	−895.33838	−893.92944		
S	−1202.42594	−1200.46612		
C−ON BDE **S** to **Nit** + π radical			BDE = 24.5	39.2
$\mathbf{SH^+_N}$	−1202.83057	−1200.86865	0.0	0.0
$\mathbf{TSH^+_{NP}}$	−1202.80748	−1200.84302	14.5	16.1
$\mathbf{SH^+_P}$	−1202.82621	−1200.86341	2.7	3.3
C−ON BDE $\mathbf{SH^+}$ to $\mathbf{NitH^+_P}$ + π radical			BDE = 52.2	65.0
$\mathbf{NitH^+_N}$	−895.64501	−894.21565	0.0	0.0
$\mathbf{NitH^+_P}$	−895.69891	−894.29084	−33.8	−47.2

[a] Geometries are optimized at the B3LYP/6-31G(d) level. [b] Basis set: 6-31G(d). [c] Basis set: cc-pvtz

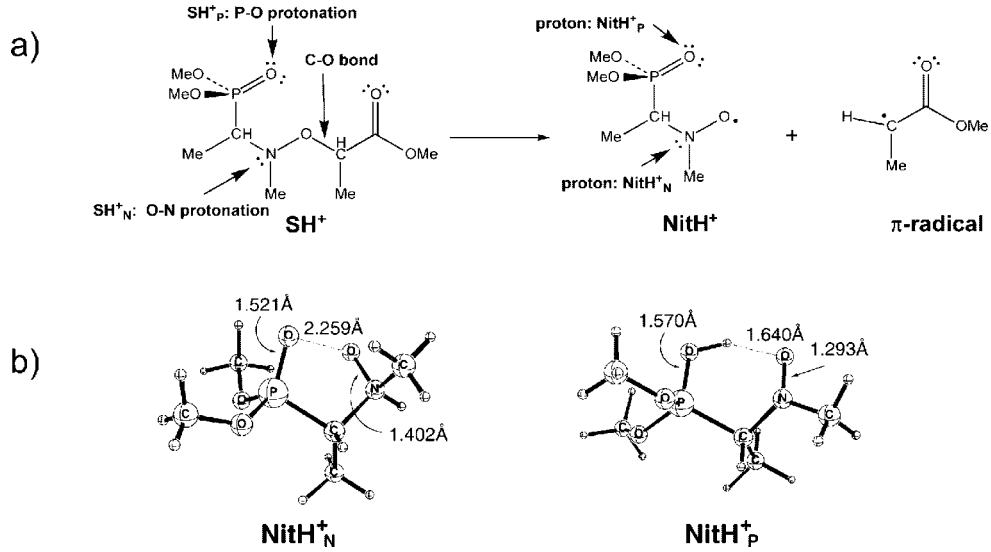

Figure 8. (a) Homolytic C−ON bond cleavage in the protonated model system (**S**) yielding a π radical and (b) B3LYP/6-31G(d)-optimized structure of the complementary protonated radicals, $\mathbf{NitH^+_P}$ and $\mathbf{NitH^+_N}$.

Scheme 3. Modelization of the Heterolytic P−C Bond Cleavage in the S Model Compound after Protonation of the Nitrogen Atom (SH^+_N), Which Would Produce a Neutral (Phos) and a Charged (Imin) Species

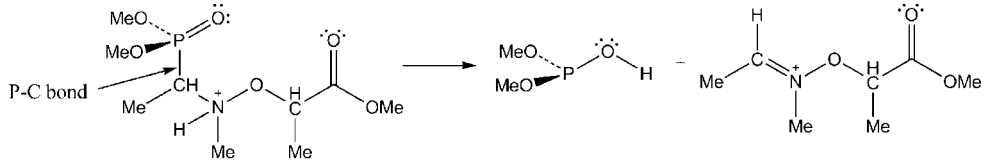

SH^+_N Phos Imin

Table 4. Energetics for the Modification of the Heterolytic P−C Bond Dissociation Energy (BDE) with Protonation

species	absolute energies (au) B3LYP[a]	PMP2[b]
	After Protonation	
SH^+_N	−1202.83057	−1200.86865
Phos	−647.47456	−646.53654
Imin(+)	−555.30450	−554.25625
BDE (kcal/mol)	32.3	47.6
	Before Protonation[c]	
S	−1202.46045	−1200.54501
Phos(-)	−646.94728	−646.01727
Imin(+)	−555.31784	−554.29827
BDE (kcal/mol)	122.6	144.0

[a] Basis set: 6-31G(d). [b] Basis set: cc-pvtz. [c] Because of the anionic phosphine fragment, standard diffuse functions were added to the basis set used for the B3LYP optimization (6-31+G(d)) and for the single point MP2 calculation aug-cc-pvtz.

about by the presence of the metal. Clearly, the slight broadening observed for carbon C-**5** (Figure 6d) cannot be due to relaxation enhancement but most probably to the chemical exchange experienced by the molecule between its bounded and free states. In any case, the observed perturbations confirm that Zn^{II} ions also bind the carboxylic group of **X**. A small effect was also observed on the C-**4** and C-**4′** carbon atoms, although no significant effect could be detected in the ^1H spectrum for the respective proton signals. Most importantly, again, no change could be evidenced for the CO-**6** atom. Finally, the absence of any effective broadening for the CH group α to the nitrogen and the phosphorus clearly excluded the involvement of these respective atoms in the metal binding process. This latter point was further supported by ^{31}P NMR experiments that did not evidence any spectral change upon the addition of divalent ions in solution (data not shown). Therefore, all of these results indicate that the hydroxyl of the carboxylic group of the MAMA moiety in **X** and $\mathbf{P_n}$ binds to divalent ions in methanol solution.

Moreover, PGSE NMR experiments were conducted to investigate the size of the complex formed in methanol-d_4 solution between Cu^{2+} or Zn^{2+} ions and **X**. The self-diffusion coefficient of **X** measured in different solutions was compared with the self-diffusion coefficient of tetramethylsilane (TMS) used as an internal reference. When aiming at estimating the relative size of compounds in solution by using NMR diffusion measurements, the use of an internal standard is especially convenient because it allows one to compensate for experimental difficulties such as pulsed-field gradients miscalibration and inhomogeneity as well as temperature and fluid viscosity changes. TMS is a particularly suitable candidate for this purpose and has been proposed for PGSE measurements in organic solvents.[56] The so-obtained D values were then used to monitor the relative change in hydrodynamic size of **X** dissolved in methanol-d_4 solutions when adding divalent (Cu^{2+}, Zn^{2+}) ions in solution. Specifically, the structural properties of the diffusing particles were related to their self-diffusion coefficient according to the Stokes−Einstein equation

$$D = \frac{kT}{6\pi\eta a} \tag{2}$$

where k is Boltzmann's constant, T is the absolute temperature, η is the solution viscosity, and a is the hydrodynamic radius. Note that this equation is strictly valid for noninteracting, spherical particles whose dimensions are much larger than those of the solvent and that undergo free diffusion in a continuous, isotropic medium. As recently emphasized by Macchioni et al.,[57] correction factors must be used to achieve more accurate results whenever the molecular shape cannot be approximated to be spherical or the particle size is comparable to that of the solvent. However, because purely qualitative results were sought here, these correction factors were not required, and the simpler eq 2 could be used. When accounting for the presence of the internal reference in solution, the application of eq 1 leads to the following relationship

$$\frac{a_X^{ref}}{a_X^{salt}} = \frac{D_{TMS}^{ref}}{D_{TMS}} \frac{D_X}{D_X^{ref}} \tag{3}$$

where $a_X^{ref}$and a_X^{salt} are the hydrodynamic radii of **X** measured in methanol-d_4 without and with added salt, and D_X^{ref}, D_X^{salt}, D_{TMS}^{ref}, and D_{TMS}^{salt} are the self-diffusion coefficients of **X** and TMS, respectively, measured in methanol-d_4 solution without and with added salt. The relative increase in the hydrodynamic size of **X** when adding divalent ions in solution can hence be estimated, as shown in Table 2. For comparison, data achieved in the presence of monovalent ions (K^+) were also reported. As can be seen, in all three cases, no significant change in molecular size could be detected within experimental error. Note that if the ratios reported in Table 2 had been different from those in Table 1, then the corresponding size increases could not have been directly used to estimate the real size of the complex in solution because the possibility of fast exchange on the diffusion time scale between the free and complexed states must also be accounted for. However, this is clearly of no concern here because our aim was merely to detect any change in molecular size qualitatively. These results suggested that when divalent ions were added to the **X** methanolic solution, the complex formed in solution between **X** and one of the divalent ions investigated here, either Cu^{II} or Zn^{II}, only involved one **X** molecule.

Role of the Proton in Collision-Induced Dissociation of PEO-MAMASG1. As shown by NMR, the displacement of the acidic proton by Cu^{2+} would lead to the formation of the $\mathbf{P_n}-H + Cu^{II}$ species in solution, further observed in ESI mass spectra as $[\mathbf{P_n}-H + Cu^{II}]^+$ and its protonated form, $[\mathbf{P_n}-H + Cu^{II} + H]^{2+}$. Because the release of SG1• was avoided only in the case of the protonated form, the key parameter for preventing homolytic cleavage of the C−ON bond would be the presence of the proton. Theoretical calculations were thus performed to evaluate the effect of protonation on the C−ON bond cleavage.

Table 5. Accurate Mass Measurements of Product Ions Formed in Collision-Induced Dissociation of Copper Adduct of the 8-mer, $[P_8 + Cu^{II}]^{2+}$, Detected at *m/z* 441.2

$(m/z)_{exp}$	Elemental composition	$(m/z)_{theo}$	Error (ppm)	Structure assignments
687.2715	$C_{29}H_{54}NO_{13}Cu^{+}$	687.2886	- 24.8	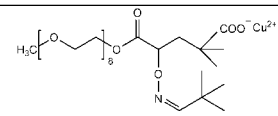
587.1982	$C_{24}H_{44}O_{12}Cu^{+\cdot}$	587.2123	- 24.1	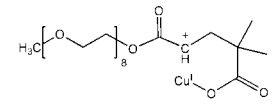
441.2015	$C_{37}H_{74}NO_{16}PCu^{2+}$	441.2015	*reference*	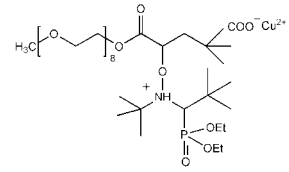
413.1686	$C_{33}H_{66}NO_{16}PCu^{2+}$	413.1702	- 3.9	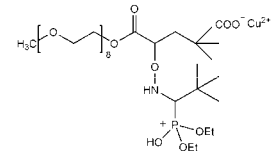
372.1789	$C_{33}H_{63}NO_{13}Cu^{2+}$	372.1792	- 0.9	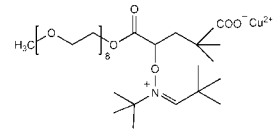
344.1478	$C_{29}H_{55}NO_{13}Cu^{2+}$	344.1479	- 0.4	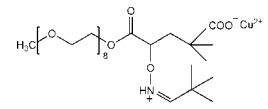
295.1885	$C_{13}H_{30}NO_4P^{+\cdot}$	295.1906	- 7.4	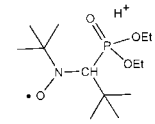
293.6058	$C_{24}H_{44}O_{12}Cu^{2+}$	293.6059	- 0.3	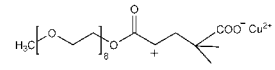
139.0527	$C_4H_{12}O_3P^{+}$	139.0518	+ 6.0	

Two protonation sites were investigated on a model of the substrate (**S**), that at the nitrogen atom of the nitroxide ($\mathbf{SH^+_N}$) and that at the oxygen of the phosphine oxide ($\mathbf{SH^+_P}$) (Figure 8a, left). The model we considered aims at reducing the conformational space and is consistent with the previous discussion about σ/π radical stability. We additionally considered the transition state to move the proton from one protonation site to the other (noted $\mathbf{TSH^+_{NP}}$). The main results are that both $\mathbf{SH^+_N}$ or $\mathbf{SH^+_P}$ can be envisaged with very similar energies and that a barrier of about 16.1 kcal/mol is to pass to move the proton from one site to the other. This means that some proton scrambling can occur between the two sites. Upon C−ON cleavage, the obtained fragments can bear the proton on either the phosphine part ($\mathbf{NitH^+_P}$) or the nitroxide ($\mathbf{NitH^+_N}$). The first is much lower in energy, with an energy difference as large as 47.2 kcal/mol (Table 3). The optimized structure for $\mathbf{NitH^+_N}$ shows a constrained five-membered ring structure (Figure 8b) with an O−O distance of 2.259 Å, a value that matches a stabilizing two-center three-electron intramolecular interaction.[58−60] Two-center three-electron bond distances are significantly exaggerated by DFT methods.[61] However, geometry should not suffer much from this in the present case because of ring constraints. Moreover, the O−O distance (2.259 Å) obtained at the B3LYP level is similar to the usual MP2-optimized O−O distance of the literature. (In the HOOH anion for instance, the optimized O−O distance is 2.248 Å at the MP2/6-31G(d) level.[62]) Similarly, Hiberty et al. have established that DFT methods heavily exaggerate the stability of this interaction, whereas the MP2 approach provides reasonably accurate results.[63,64] The PMP2 energy of the dissociate fragments should thus be sufficiently accurate for discussing the present fragmentations on an equal footing. Using this level, it is noteworthy (Table 3) that the C−ON bond dissociation energy increases by about 25 kcal upon protonation (39.2 vs 65.0 kcal/mol). Upon nitrogen protonation, the P−C bond can also be broken,[65] as described in Scheme 3. Such a bond cleavage would involve the aforementioned proton migration from the nitrogen to the phosphine oxide ($E^{\#}$ = 16.1 kcal/mol). The computed values

show that the total energy of such a process would require 47.6 kcal/mol (Table 4). This value is significantly lower than that of the corresponding C−ON bond (65.0 kcal/mol). As a result, the P−C bond would be easier to cleave than the C−ON bond when the substrate is protonated.

Dissociation pathways of *m/z* 441.2 in Figure 3b were then studied from the ionic structure of $[\mathbf{P_8} + Cu^{II}]^{2+}$ revealed by NMR and theoretical calculations. Both accurate mass measurements (Table 5) and MS/MS experiments on $[\mathbf{P_8} + {}^{65}Cu^{II}]^{2+}$ at *m/z* 442.2 (data not shown) were performed to support the proposed dissociation pathways. Considering that the proton is located on the N atom, the precursor ion would dissociate according to two main pathways, as previously reported in a recent study.[22] Protonation of the O atom in the phosphine group would occur (i) in a 1,6-proton transfer to allow the release of a 2-methylprop-1-ene molecule and the production of *m/z* 413.2 and (ii) in a 1,4-mechanism to yield *m/z* 372.2 and a neutral diethylhydrogen phosphite. Two fragmentation pathways could be proposed to account for the production of *m/z* 344.1. The heterolytic cleavage of the C−P bond in *m/z* 413.2 would allow the phosphorus atom oxidation state to be reduced, inducing the elimination of a neutral diethylhydrogen phosphite and the formation of *m/z* 344.1. Alternatively, a 1,3-proton transfer from a methyl group to the nitrogen atom in *m/z* 372.2 would allow the same *m/z* 344.1 ion to be produced after the elimination of a 2-methylprop-1-ene molecule.

The formation of *m/z* 293.6 would result from a concerted electron migration induced by protonation of the oxygen of the phosphine group, giving rise to the elimination of two neutrals, namely, 1,1-dimethylnitrosoethane and diethylhydrogen-2,2-dimethylpropylidene phosphate. A very low abundance peak, detected at *m/z* 295.2 in the MS/MS spectrum and assigned to protonated SG1• on the basis of accurate mass measurements, would indicate that the homolytic cleavage of the C−ON bond in the oligomer end group actually occurred at a very small extent. The complementary ion produced in this dissociation reaction, namely, $[\mathbf{P_8}-SG1\bullet + Cu^{II}]^{+}$, was also detected at *m/z* 587.2. Finally, although detected as a singly charged molecule, the ion at *m/z* 687.3 would contain copper as Cu^{II} (i.e., no reduction in the copper oxidation state has occurred) and would result from the dissociation of *m/z* 413.2, proceeding via a 1,6 proton transfer that would also give rise to a protonated diethyl phosphonate observed with a very low abundance at *m/z* 139.1. CID experiments carried out for $[\mathbf{P_n} + 2H]^{2+}$ ions produced from acidified polymer solution (data not shown) indicate that the same fragmentation pathways were involved during the dissociation of the doubly protonated oligomers, which further supports the proposed charge-induced fragmentation mechanisms.

Conclusions

Among the tested cationizing agents, divalent cations such as Cu^{2+}, Zn^{2+}, and Ca^{2+} were shown to promote selective protonation of the PEO-MAMASG1 end group and thus prevent the labile nitroxide moiety to be released upon CID. As suggested by NMR results combined with theoretical calculations, divalent cations would induce an internal proton transfer from the acidic group of the MAMA to atoms in the SG1 part. In contrast, oligomers adducted with alkali cations were all shown to dissociate readily via the homolytic cleavage of the fragile C−ON bond, suggesting that alkali were preferentially bound to oxygen atoms in the PEO chain.[66,67] The propensity of divalent cations to favor the same protonation mechanism in MALDI and thus to allow intact oligomer ions to be detected is currently under investigation.

The reported multidisciplinary approach also allowed us to reach new insight into the actual role of the proton in preventing the fragmentation of labile end groups. According to theoretical calculations, the C−ON bond would not be the weakest bond once the N atom of the nitroxide or the O atom of the phosphine oxide within the end group is protonated. As a result, the reaction involving the release of the nitroxide radical would no longer efficiently compete with alternative dissociation pathways.

Acknowledgment. This work was supported by the French Research Agency (ANR-06-JCJC-0112). L.C. and S.V. acknowledge support from Spectropole, the Analytical Facility of Aix-Marseille University, by allowing special access to the instruments purchased with European Funding (FEDER OBJ2142-3341). S.H. acknowledges support from the Centre Régional de Compétences en Modélisation Moléculaire de Marseille, The Computing Facility of Aix-Marseille University. T.N.T.P. acknowledges Arkema for kindly supplying the MAMASG1 alkoxyamine.

Supporting Information Available: Electrospray mass spectra of PEO-MAMA-SG1 using lithium and sodium as the cationing agent, complete ref 35, and complete computational results (geometries, energies, $<S^2>$ values). This material is available free of charge via the Internet at http://pubs.acs.org.

References and Notes

(1) Park, C.; Yoon, J.; Thomas, E. L. *Polymer* **2003**, *44*, 6725–6760.
(2) Hadjichristidis, N.; Pispas, S.; Floudas, G. A. *Block Copolymers: Synthetic Strategies, Physical Properties, and Applications*; Wiley-Interscience: New York, 2003.
(3) Hamley, I. W. *The Physics of Block Copolymers*; Oxford University Press: Oxford, U.K., 1998.
(4) Tirelli, N.; Lutolf, M. P.; Napoli, A.; Hubbell, J. A. *Rev. Mol. Biotechnol.* **2002**, *90*, 3–15.
(5) Mawson, S.; Yates, M. Z.; Oneill, M. L.; Johnston, K. P. *Langmuir* **1997**, *13*, 1519–1528.
(6) Sakai, T.; Alexandridis, P. *Langmuir* **2004**, *20*, 8426–8430.
(7) Jeon, H. J.; Go, D. H.; Choi, S. Y.; Kim, K. M.; Lee, J. Y.; Choo, D. J.; Yoo, H. O.; Kim, J. M.; Kim, J. *Colloids Surf., A* **2008**, *317*, 496–503.
(8) Bloch, E.; Phan, T.; Bertin, D.; Llewellyn, P.; Hornebecq, V. *Microporous Mesoporous Mater.* **2008**, *112*, 612–620.
(9) Singh, M.; Odusanya, O.; Wilmes, G. M.; Eitouni, H. B.; Gomez, E. D.; Patel, A. J.; Chen, V. L.; Park, M. J.; Fragouli, P.; Iatrou, H.; Hadjichristidis, N.; Cookson, D.; Balsara, N. P. *Macromolecules* **2007**, *40*, 4578–4585.
(10) Guilherme, L. A.; Borges, R. S.; Moraes, E. M. S.; Silva, G. G.; Pimenta, M. A.; Marletta, A.; Silva, R. A. *Electrochim. Acta* **2007**, *53*, 1503–1511.
(11) Sinturel, C.; Vayer, M.; Erre, R.; Amenitsch, H. *Macromolecules* **2007**, *40*, 2532–2538.
(12) Guo, Q. P. *Thermochim. Acta* **2006**, *451*, 168–173.
(13) Huang, P.; Zhu, L.; Cheng, S. Z. D.; Ge, Q.; Quirk, R. P.; Thomas, E. L.; Lotz, B.; Hsiao, B. S.; Liu, L. Z.; Yeh, F. J. *Macromolecules* **2001**, *34*, 6649–6657.
(14) *Controlled/Living Radical Polymerization: Progress in ATRP, NMP, and RAFT*; Matyjaszewski, K., Ed.; ACS Symposium Series 768; American Chemical Society: Washington, DC, 2000.
(15) Barner-Kowollik, C.; Davis, T. P.; Stenzel, M. H. *Polymer* **2004**, *45*, 7791–7805.
(16) Beyou, E.; Chaumont, P.; Chauvin, F.; Devaux, C.; Zydowicz, N. *Macromolecules* **1998**, *31*, 6828–6835.
(17) Gruendling, T.; Hart-Smith, G.; Davis, T. P.; Stenzel, M. H.; Barner-Kowollik, C. *Macromolecules* **2008**, *41*, 1966–1971.
(18) Jiang, X. L.; Schoenmakers, P. J.; van Dongen, J. L. J.; Lou, X. W.; Lima, V.; Brokken-Zijp, J. *Anal. Chem.* **2003**, *75*, 5517–5524.
(19) Bartsch, A.; Dempwolf, W.; Bothe, M.; Flakus, S.; Schmidt-Naake, G. *Macromol. Rapid Commun.* **2003**, *24*, 614–619.
(20) Dourges, M. A.; Charleux, B.; Vairon, J. P.; Blais, J. C.; Bolbach, G.; Tabet, J. C. *Macromolecules* **1999**, *32*, 2495–2502.
(21) Schulte, T.; Siegenthaler, K. O.; Luftmann, H.; Letzel, M.; Studer, A. *Macromolecules* **2005**, *38*, 6833–6840.
(22) Mazarin, M.; Phan, T. N. T.; Charles, L. *Rapid Commun. Mass Spectrom.* **2008**, *22*, 3776–3782.
(23) D'Agosto, F.; Hughes, R.; Charreyre, M. T.; Pichot, C.; Gilbert, R. G. *Macromolecules* **2003**, *36*, 621–629.
(24) Ganachaud, F.; Monteiro, M. J.; Gilbert, R. G.; Dourges, M. A.; Thang, S. H.; Rizzardo, E. *Macromolecules* **2000**, *33*, 6738–6745.

(25) Schilli, C.; Lanzendorfer, M. G.; Muller, A. H. E. *Macromolecules* **2002**, *35*, 6819–6827.
(26) Llenes, C. F.; Omalley, R. M. *Rapid Commun. Mass Spectrom.* **1992**, *6*, 564–570.
(27) Polce, M. J.; Ocampo, M.; Quirk, R. P.; Leigh, A. M.; Wesdemiotis, C. *Anal. Chem.* **2008**, *80*, 355–362.
(28) Polce, M. J.; Ocampo, M.; Quirk, R. P.; Wesdemiotis, C. *Anal. Chem.* **2008**, *80*, 347–354.
(29) Girod, M.; Phan, T. N. T.; Charles, L. *J. Am. Soc. Mass Spectrom.* **2008**, *19*, 1163–1175.
(30) Berger, S.; Braun, S. *200 and More NMR Experiments: A Practical Course*; Wiley-VCH: Weinheim, Germany, 2005; pp 1−854.
(31) Antalek, B. *Concepts Magn. Reson.* **2002**, *14*, 225–258.
(32) Price, W. S. *Concepts Magn. Reson.* **1998**, *10*, 197–237.
(33) Stilbs, P. *Prog. Nucl. Magn. Reson. Spectrosc.* **1987**, *19*, 1–45.
(34) Wu, D.; Chen, A.; Johnson, C. S., Jr. *J. Magn. Reson., Ser. A* **1995**, *115*, 260–264.
(35) Frisch, M. J.; Trucks, G. W.; Schlegel, H. B.; Scuseria, G. E.; Robb, M. A.; Cheeseman, J. R.; Montgomery, J. A., Jr.; Vreven, T.; Kudin, K. N.; Burant, J. C.; Millam, J. M.; Iyengar, S. S.; Tomasi, J.; Barone, V.; Mennucci, B.; Cossi, M.; Scalmani, G.; Rega, N.; Petersson, G. A.; Nakatsuji, H.; Hada, M.; Ehara, M.; Toyota, K.; Fukuda, R.; Hasegawa, J.; Ishida, M.; Nakajima, T.; Honda, Y.; Kitao, O.; Nakai, H.; Klene, M.; Li, X.; Knox, J. E.; Hratchian, H. P.; Cross, J. B.; Bakken, V.; Adamo, C.; Jaramillo, J.; Gomperts, R.; Stratmann, R. E.; Yazyev, O.; Austin, A. J.; Cammi, R.; Pomelli, C.; Ochterski, J. W.; Ayala, P. Y.; Morokuma, K.; Voth, G. A.; Salvador, P.; Dannenberg, J. J.; Zakrzewski, V. G.; Dapprich, S.; Daniels, A. D.; Strain, M. C.; Farkas, O.; Malick, D. K.; Rabuck, A. D.; Raghavachari, K.; Foresman, J. B.; Ortiz, J. V.; Cui, Q.; Baboul, A. G.; Clifford, S.; Cioslowski, J.; Stefanov, B. B.; Liu, G.; Liashenko, A.; Piskorz, P.; Komaromi, I.; Martin, R. L.; Fox, D. J.; Keith, T.; Al-Laham, M. A.; Peng, C. Y.; Nanayakkara, A.; Challacombe, M.; Gill, P. M. W.; Johnson, B.; Chen, W.; Wong, M. W.; Gonzalez, C.; Pople, J. A. Gaussian 03, revision C.02; Gaussian, Inc.: Wallingford, CT, 2004.
(36) Woon, D. E.; Dunning, T. H. *J. Chem. Phys.* **1993**, *98*, 1358–1371.
(37) Davidson, E. R. *Chem. Phys. Lett.* **1996**, *260*, 514–518.
(38) Lattimer, R. P. *J. Am. Soc. Mass Spectrom.* **1992**, *3*, 225–234.
(39) Williams, J. P.; Hilton, G. R.; Thalassinos, K.; Jackson, A. T.; Scrivens, J. H. *Rapid Commun. Mass Spectrom.* **2007**, *21*, 1693–1704.
(40) Lattimer, R. P. *J. Am. Soc. Mass Spectrom.* **1994**, *5*, 1072–1080.
(41) Chen, R.; Li, L. *J. Am. Soc. Mass Spectrom.* **2001**, *12*, 832–839.
(42) Hoteling, A. J.; Kawaoka, K.; Goodberlet, M. C.; Yu, W. M.; Owens, K. G. *Rapid Commun. Mass Spectrom.* **2003**, *17*, 1671–1676.
(43) Jackson, A. T.; Green, M. R.; Bateman, R. H. *Rapid Commun. Mass Spectrom.* **2006**, *20*, 3542–3550.
(44) Okuno, S.; Kiuchi, M.; Arakawa, R. *Eur. J. Mass Spectrom.* **2006**, *12*, 181–187.
(45) Selby, T. L.; Wesdemiotis, C.; Lattimer, R. P. *J. Am. Soc. Mass Spectrom.* **1994**, *5*, 1081–1092.
(46) Girod, M.; Carissan, Y.; Humbel, S.; Charles, L. *Int. J. Mass Spectrom.* **2008**, *272*, 1–11.
(47) Charles, L. *Rapid Commun. Mass Spectrom.* **2008**, *22*, 151–155.
(48) Dempwolf, W.; Flakus, S.; Schmidt-Naake, G. *Macromol. Symp.* **2007**, *259*, 416–420.
(49) Deery, M. J.; Jennings, K. R.; Jasieczek, C. B.; Haddleton, D. M.; Jackson, A. T.; Yates, H. T.; Scrivens, J. H. *Rapid Commun. Mass Spectrom.* **1997**, *11*, 57–62.
(50) Bertin, D.; Gigmes, D.; Marque, S. R. A.; Tordo, P. *Macromolecules* **2005**, *38*, 2638–2650.
(51) Fischer, H.; Kramer, A.; Marque, S. R. A.; Nesvadba, P. *Macromolecules* **2005**, *38*, 9974–9984.
(52) Bertin, D.; Gigmes, D.; Marque, S. R. A.; Siri, D.; Tordo, P.; Trappo, G. *ChemPhysChem* **2008**, *9*, 272–281.
(53) Marque, S.; Le Mercier, C.; Tordo, P.; Fischer, H. *Macromolecules* **2000**, *33*, 4403–4410.
(54) Torreggiani, A.; Fini, G.; Bottura, G. *J. Mol. Struct.* **2001**, *565*, 341–346.
(55) Farrar, T. C.; Becker, E. D. *Pulse and Fourier Transform NMR: Introduction to Theory and Methods*; Academic Press: New York, 1971; p 115.
(56) Cabrita, E.; Berger, S. *Magn. Reson. Chem.* **2001**, *39*, S142–S148.
(57) Macchioni, A.; Ciancaleoni, G.; Zuccaccia, C.; Zuccaccia, D. *Chem. Soc. Rev.* **2008**, *37*, 479–489.
(58) Baird, N. C. *J. Chem. Educ.* **1977**, *54*, 291–293.
(59) Humbel, S.; Hiberty, P. C. *THEOCHEM* **1998**, *424*, 57–65.
(60) Symons, M. C. R.; Wren, B. W. *J. Chem. Soc., Perkin Trans. 2* **1984**, *3*, 511–522.
(61) Braida, B.; Hiberty, P. C.; Savin, A. *J. Phys. Chem. A* **1998**, *102*, 7872–7877.
(62) Humbel, S.; Demachy, I.; Hiberty, P. C. *Chem. Phys. Lett.* **1995**, *247*, 126–134.
(63) Hiberty, P. C.; Humbel, S.; Danovich, D.; Shaik, S. *J. Am. Chem. Soc.* **1995**, *117*, 9003–9011.
(64) Braida, B.; Lauvergnat, D.; Hiberty, P. C. *J. Chem. Phys.* **2001**, *115*, 90–102.
(65) Doskocz, M.; Roszak, S.; Majumdar, D.; Doskocz, J.; Gancarz, R.; Leszczynski, J. *J. Phys. Chem. A* **2008**, *112*, 2077–2081.
(66) Vonhelden, G.; Wyttenbach, T.; Bowers, M. T. *Science* **1995**, *267*, 1483–1485.
(67) Wu, J. L.; Polce, M. J.; Wesdemiotis, C. *J. Am. Chem. Soc.* **2000**, *122*, 12786–12794.

MA802372M